
Non-negative Tensor Mixture Learning for Discrete Density Estimation

Kazu Ghalamkari

RIKEN AIP

kazu.ghalamkari@riken.jp

Jesper Løve Hinrich

Technical University of Denmark

jehi@dtu.dk

Morten Mørup

Technical University of Denmark

mmor@dtu.dk

Abstract

We present an expectation-maximization (EM) based unified framework for non-negative tensor decomposition that optimizes the Kullback-Leibler divergence. To avoid iterations in each M-step and learning rate tuning, we establish a general relationship between low-rank decomposition and many-body approximation. Using this connection, we exploit that the closed-form solution of the many-body approximation can be used to update all parameters simultaneously in the M-step. Our framework not only offers a unified methodology for a variety of low-rank structures, including CP, Tucker, and Train decompositions, but also their combinations forming mixtures of tensors as well as robust adaptive noise modeling. Empirically, we demonstrate that our framework provides superior generalization for discrete density estimation compared to conventional tensor-based approaches.

1 Introduction

In machine learning, a key aim of unsupervised learning is to perform accurate density estimation of high-dimensional data. The estimated density can then be used for multiple purposes such as predicting new data points, inferring missing values, performing outlier detection, or generating new data points for data augmentation. Density estimation has typically been addressed by the use of parametric and non-parametric methodologies, including mixture modeling approaches and kernel density estimation procedures [22]. Recently, deep learning-based models have been found to accurately characterize the underlying data distribution by use of variational auto-encoders, auto-regressive, as well as flow and diffusion-based generative models; for an overview, see [26].

In this paper, we focus on discrete density estimation which seeks to characterize the joint distribution $P(x_1, \dots, x_D)$ where each discrete random variable $x_d \in \{1, 2, \dots, I_d\}$ corresponds to a categorical feature. Such discrete distributions are naturally identical to normalized non-negative *tensors*, or multidimensional arrays. A series of recent studies estimate the discrete distribution behind categorical data [10, 19] by approximating a tensor constructed from the observed data, i.e., the *empirical tensor*, with a low-rank tensor described by a linear combination of a small number of bases; however, two challenges remain in these current works.

The first challenge is to develop a unified formulation of nonnegative tensor decomposition that works with various kinds of low-rank structures, optimizing the Kullback–Leibler (KL) divergence, which is a natural measure of similarity between probability distributions. In contrast to the well-

established SVD-based methods for real- and complex-valued tensor networks [5, 13, 20], a general framework for nonnegative tensor decompositions optimizing the KL divergence is not well developed. Consequently, some existing studies of tensor-based discrete density estimation have been performed via optimization of the Frobenius norm, which imposes unnatural modeling assumptions when applied to probability distributions [19]. In addition, due to the lack of a unified KL-divergence-based framework, users can try only popular low-rank structures that have been developed piecemeal or differentiate the cost function for each low-rank structure by themselves. A framework that allows users to try various low-rank structures more intuitively and freely is, therefore, desirable.

The second challenge is scalability, as the size of the tensor — which corresponds to the sample space size of the discrete distribution — increases exponentially with the number of features D , namely a tensor has I^D elements for the degree of freedom of each feature I . However, the number of samples available for training N — typically indicates the number of nonzero values of the empirical tensor — is often limited, also deemed the curse of dimensionality. Therefore, it is desirable to develop scalable tensor decomposition methods that can operate well for high-dimensional data despite a limited number of samples available.

To address these two challenges, this paper proposes a unified non-negative tensor factorization method based on the expectation-maximization (EM) algorithm [7]. The EM algorithm is an iterative framework for maximum likelihood estimation that repeatedly maximizes the lower bound of the log-likelihood function in two steps, the E-step and the M-step. The naive formulation of the EM-based general non-negative tensor decomposition requires either an alternating optimization bounding the log-likelihood (E-step) and maximizing (M-step) each factor at a time or gradient methods in each M-step. It requires either tailoring methods to each type of decomposition or time-consuming double iterative methods. To overcome this issue, we exploit that the optimization required in each M-step coincides with a tensor many-body approximation [9] that decomposes tensors by a reduced representation of the interactions among tensor modes. We derive the exact closed-form solution for many-body approximation that appears in EM algorithms for Tucker and Train decomposition, and thereby successfully remove the gradient method in M-step for various kinds of low-rank approximation by combining these two closed-form formulas.

Our framework inherits the properties of the EM algorithm [27], and therefore, it always converges regardless of the choice of the low-rank structure assumed in the model. Furthermore, the tensor to be approximated in the M-step is sparse as it is defined in terms of elementwise multiplications by the empirical tensor. As a result, the computational complexity of the proposed method is proportional to the number of observations N . Notably, as the EM algorithm is frequently used for maximum likelihood estimation of mixture models, the proposed method allows for density estimation using mixtures of low-rank tensor decompositions providing a flexible modeling framework that has not been studied previously. We empirically show that learning such tensor mixtures provides better generalization than pure low-rank tensor models for discrete density estimation. We summarize our contribution as follows:

- We reveal a relationship between tensor many-body approximation and traditional low-rank approximation.
- Using this relationship, we provide a unified EM-based framework for non-negative low-rank approximation optimizing the KL-divergence, notably providing simultaneous closed-form updates for all parameters in the M-step while exploiting the sparsity structure of the empirically estimated joint distribution.
- Based on the proposed framework, we develop a mixture of low-rank tensor modeling approach that empirically demonstrates inferential robustness and improved generalization.

2 Low-rank approximation and many-body approximation

The naive direct EM-based formulation for non-negative low-rank approximation bounding the likelihood in the E-step and optimizing all parameters in the M-step relies on an iterative gradient method in the M-step. We presently explore the relationship between low-rank decomposition and many-body approximation and leverage that the many-body approximation provides exact closed-form solutions to eliminate the gradient method in the M-step. We describe in Section 2.2 that the marginalization along the tensor modes connects many-body approximation to low-rank decomposition.

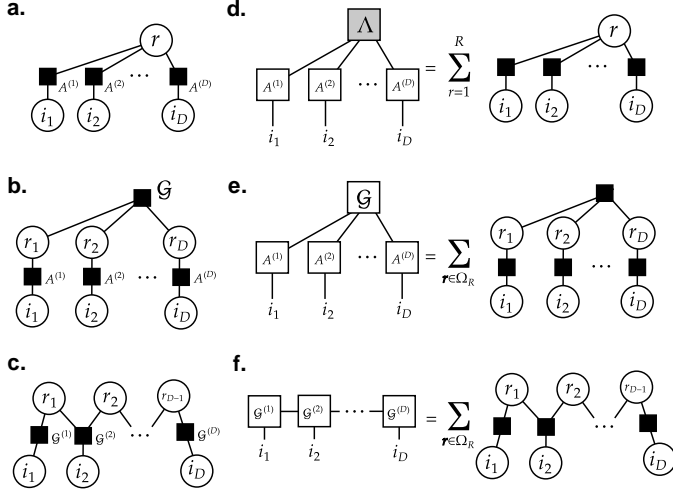


Figure 1: **(a,b,c)** Interaction diagrams for tensors Q^{CP} , Q^{Tucker} , and Q^{Train} , respectively, in Equation (1). Each node represents a tensor mode, and the black square, \blacksquare , represents the interaction between modes. **(d,e,f)** Tensor networks for \mathcal{P}^{CP} , $\mathcal{P}^{\text{Tucker}}$, and $\mathcal{P}^{\text{Train}}$, respectively, in Equation (6). Nodes represent factor tensors, and edges represent mode products. The gray-filled Λ is a tensor whose hyper-diagonal elements are 1 otherwise 0. These low-rank tensors correspond to marginalizations of \mathbf{r} modes in the many-body approximation.

2.1 Many-body approximation with exact closed-form solution

Many-body approximation factorizes tensors by given interactions among tensor modes. These interactions are described through an interaction diagram, as shown in Figure 1. Each node (circle) corresponds to a tensor index and edges through a black square, \blacksquare , mean the existence of interaction. In the following, we denote by $[d] = \{1, 2, \dots, d\}$ for a positive integer d . We provide three examples, a $(D + 1)$ -th order tensor $Q^{\text{CP}} \in \mathbb{R}_{\geq 0}^{I_1 \times \dots \times I_D \times R}$, a $2D$ -th order tensor $Q^{\text{Tucker}} \in \mathbb{R}_{\geq 0}^{I_1 \times \dots \times I_D \times R_1 \times \dots \times R_D}$, and a $(2D - 1)$ -th order tensor $Q^{\text{Train}} \in \mathbb{R}_{\geq 0}^{I_1 \times \dots \times I_D \times R_1 \times \dots \times R_{D-1}}$. When their interactions are described as Figure 1(a), (b), and (c) respectively, they can be factorized as

$$Q_{i_1 \dots i_D r}^{\text{CP}} = \prod_{d=1}^D A_{i_d r}^{(d)}, \quad Q_{i_1 \dots i_D r_1 \dots r_D}^{\text{Tucker}} = \mathcal{G}_{r_1 \dots r_D} \prod_{d=1}^D A_{i_d r_d}^{(d)}, \quad Q_{i_1 \dots i_D r_1 \dots r_{D-1}}^{\text{Train}} = \prod_{d=1}^D \mathcal{G}_{r_{d-1} i_d r_d}^{(d)}, \quad (1)$$

where $i_d \in [I_d]$ and $r_d \in [R_d]$ for $d = 1, \dots, D$. For simplicity, we suppose $r_0 = r_D = 1$ for Q^{Train} . Let tensor indices i_1, \dots, i_D and r_1, \dots, r_V be \mathbf{i} and \mathbf{r} , respectively. Here, the integer V is 1 for Q^{CP} , D for Q^{Tucker} , and $D - 1$ for Q^{Train} . We denote the domains of \mathbf{i} and \mathbf{r} by Ω_I and Ω_R , respectively, i.e., $\mathbf{i} \in \Omega_I = [I_1] \times \dots \times [I_D]$ and $\mathbf{r} \in \Omega_R = [R_1] \times \dots \times [R_V]$. The symbol Ω with upper indices refers to the index set for all indices other than the upper indices, e.g.,

$$\Omega_I^d = [I_1] \times \dots \times [I_{d-1}] \times [I_{d+1}] \times \dots \times [I_D], \\ \Omega_R^{d,d-1} = [R_1] \times \dots \times [R_{d-2}] \times [R_{d+1}] \times \dots \times [R_V].$$

Many-body approximation parameterizes tensors as discrete distributions, where the random variables correspond to the tensor modes, and the sample space corresponds to the index set of a tensor. Maximum likelihood estimation then finds the globally optimal tensor that minimizes the cross-entropy from the data tensor \mathcal{M} to the tensor in the model space \mathcal{B} , which is the set of tensors with specific interactions. Thus, for a given tensor \mathcal{M} , the many-body approximation based on the above three interactions maximizes

$$L_{\text{MBA}}(\mathcal{M}; Q^k) = \sum_{\mathbf{i} \in \Omega_I} \sum_{\mathbf{r} \in \Omega_R} \mathcal{M}_{\mathbf{i}\mathbf{r}} \log Q_{\mathbf{i}\mathbf{r}}^k, \quad k \in \{\text{CP}, \text{Tucker}, \text{Train}\}. \quad (2)$$

This optimization is equivalent to optimizing the KL divergence from tensor \mathcal{M} to Q^k and is guaranteed to be a convex problem regardless of the choice of interaction. While the conventional method finds a numerical solution of general many-body approximation by the Natural gradient method, it has been shown in [12] that the following factors globally maximize $L_{\text{MBA}}(\mathcal{M}; Q^{\text{CP}})$:

$$A_{i_d r}^{(d)} = \frac{\sum_{\mathbf{i} \in \Omega_I^d} \mathcal{M}_{\mathbf{i}\mathbf{r}}}{\mu^{1/D} \left(\sum_{\mathbf{i} \in \Omega_I^d} \mathcal{M}_{\mathbf{i}\mathbf{r}} \right)^{1-1/D}}, \quad \mu = \sum_{\mathbf{i} \in \Omega_I} \sum_{\mathbf{r} \in \Omega_R} \mathcal{M}_{\mathbf{i}\mathbf{r}}, \quad (3)$$

which is consistent with mean-field approximation [8]. As a generalization of the above result, we presently provide the optimal solution of the many-body approximation of Q^{Tucker} and Q^{Train} in closed-form. The following tensors globally maximizes $L_{\text{MBA}}(\mathcal{M}; Q^{\text{Tucker}})$:

$$\mathcal{G}_r = \frac{\sum_{i \in \Omega_I} \mathcal{M}_{ir}}{\sum_{i \in \Omega_I} \sum_{r \in \Omega_R} \mathcal{M}_{ir}}, \quad A_{i_d r_d}^{(d)} = \frac{\sum_{i \in \Omega_I^d} \sum_{r \in \Omega_R^d} \mathcal{M}_{ir}}{\sum_{i \in \Omega_I} \sum_{r \in \Omega_R^d} \mathcal{M}_{ir}}, \quad (4)$$

and following tensors globally maximizes $L_{\text{MBA}}(\mathcal{M}; Q^{\text{Train}})$:

$$\mathcal{G}_{r_{d-1} i_d r_d}^{(d)} = \frac{\sum_{i \in \Omega_I^d} \sum_{r \in \Omega_R^{d,d-1}} \mathcal{M}_{ir}}{\sum_{i \in \Omega_I} \sum_{r \in \Omega_R^d} \mathcal{M}_{ir}}, \quad (5)$$

where we assume $r_0 = r_D = 1$. We formally derive the above closed-form solutions in Theorems 2 and 3 in the supplementary material. Notably, we can obtain exact solutions also for more complicated many-body approximations by combining these solutions, which we discuss in Section 3.3.

2.2 Many-body approximation and low-rank approximation

When summing the tensors in Equation (1) over indices \mathbf{r} , these models are identical to the traditional low-rank models based on CP, Tucker, and Tensor Train formats, respectively.

$$\mathcal{P}_i^{\text{CP}} = \sum_r \mathcal{Q}_{ir}^{\text{CP}}, \quad \mathcal{P}_i^{\text{Tucker}} = \sum_{r_1 \dots r_D} \mathcal{Q}_{ir_1 \dots r_D}^{\text{Tucker}}, \quad \mathcal{P}_i^{\text{Train}} = \sum_{r_1 \dots r_{D-1}} \mathcal{Q}_{ir_1 \dots r_{D-1}}^{\text{Train}}. \quad (6)$$

Since many-body approximation treats the tensor indices as discrete random variables, we consider these low-rank tensors as models in which the random variables i and \mathbf{r} represent visible and hidden variables, respectively. The degree of freedom of hidden variables (R_1, \dots, R_V) corresponds to *CP rank*, *Tucker rank*, and *train rank* with $V = 1$ for Q^{CP} , $V = D$ for Q^{Tucker} , and $V = D - 1$ for Q^{Train} , respectively. Since any low-rank factorization decomposes a tensor by summing over its ranks, *any low-rank approximation can be regarded as a many-body approximation with hidden variables*. When a low-rank tensor \mathcal{P} is obtained by marginalization of a tensor \mathcal{Q} with appropriately selected modes, we refer to tensor \mathcal{Q} as the *low-body tensor* corresponding to \mathcal{P} . For example, Q^{CP} , Q^{Tucker} and Q^{Train} are low-body tensors corresponding to a low CP-rank tensor, low Tucker-rank tensor, and low Train-rank tensor, respectively. In this paper, hidden variables — corresponding to modes summed according to the low-rank structure — are denoted by \mathbf{r} and visible variables — variables other than hidden variables — by i .

The many-body approximation involves only visible variables in the model, making maximum likelihood estimation a convex optimization problem, while a low-rank approximation becomes a nonconvex optimization problem due to the marginalized hidden variables in the model. Therefore, although finding an exact solution for the low-rank approximation is challenging, the optimization remains tractable through the EM algorithm [7], a well-known general framework for maximum likelihood estimation that accommodates hidden variables.

Whereas it is already known that many-body approximation coincides with the non-negative tensor network using Dirac tensors on the nodes [9], it is our contribution to clarify the relationship between general low-rank approximation and many-body approximation.

3 Discrete density estimation via non-negative tensor learning

Based on the exact solutions of many-body approximation, we develop a novel framework *EM non-negative tensor learning* for discrete density estimation. We construct a normalized histogram, or empirical distribution, from tabular data with D categorical features. This histogram is identical to a normalized D -th order tensor $\mathcal{T} \in \mathbb{R}_{\geq 0}^{I_1 \times \dots \times I_D}$ where I_d is the degree of freedom (i.e., categories) of the d -th categorical feature. The number of non-zero values in the tensor is equivalent to the number of observed samples N if there is no identical sample in the data. To estimate the discrete probability distribution underlying the data, we approximate such a tensor \mathcal{T} with a low-rank mixture \mathcal{P} , which is a convex linear combination of K low-rank tensors.

Our framework has two advantages: (1) it achieves linear computational complexity relative to the number of nonzero elements in the input tensor, as described in Section 3.2; and (2) it has the

flexibility to generalize complicated low-rank structures and adaptive regularization terms without losing the convexity of the E and M-step, as detailed in Sections 3.3 and 3.4. Neither of these advantages has been explored in previous studies [10, 12].

3.1 EM-method for mixture of low-rank approximations

Here, we provide a unified EM-based method for a mixture of low-rank approximations. We maximize the negative cross-entropy from a given D -th order tensor \mathcal{T} to a mixture of K low-rank tensors $\mathcal{P}^1, \dots, \mathcal{P}^K$,

$$L(\hat{\mathcal{Q}}) = \sum_{i \in \Omega_I} \mathcal{T}_i \log \sum_{k=1}^K \eta^k \mathcal{P}_i^k, \quad \mathcal{P}_i^k = \sum_{\mathbf{r} \in \Omega_{R^k}} \mathcal{Q}_{i\mathbf{r}}^k, \quad (7)$$

where the mixture ratio satisfies $\sum_k \eta^k = 1$ and $\eta^k \geq 0$ for all $k \in [K]$ and setting $K = 1$ yields a conventional low-rank tensor decomposition. Each low-rank tensor \mathcal{P}^k is normalized, i.e., $\sum_i \mathcal{P}_i^k = 1$. We let the model \mathcal{P} be the convex linear combination of low-rank tensors, that is, $\mathcal{P} = \sum_k \eta^k \mathcal{P}^k$. We denote the number of hidden variables in the tensor \mathcal{Q}^k by V^k , and $\mathbf{r} \in \Omega_{R^k} = [R_1^k] \times \dots \times [R_{V^k}^k]$. For simplicity, we introduce $\hat{\mathcal{Q}}_{i\mathbf{r}}^k = \eta^k \mathcal{Q}_{i\mathbf{r}}^k$, and refer to the tensors $\hat{\mathcal{Q}}^1, \dots, \hat{\mathcal{Q}}^K$ as $\hat{\mathcal{Q}}$. We apply Jensen's inequality [14] to the objective function $L(\hat{\mathcal{Q}})$ in order to move the summation over hidden variables \mathbf{r} outside the logarithm function thereby obtaining the lower bound,

$$L(\hat{\mathcal{Q}}) \geq \bar{L}(\hat{\mathcal{Q}}, \Phi) = \sum_{i \in \Omega_I} \sum_{k=1}^K \sum_{\mathbf{r} \in \Omega_{R^k}} \mathcal{T}_i \Phi_{i\mathbf{r}}^k \log \frac{\hat{\mathcal{Q}}_{i\mathbf{r}}^k}{\Phi_{i\mathbf{r}}^k} \quad (8)$$

for any K tensors $\Phi = (\Phi^1, \dots, \Phi^K)$ where Φ^k is a $(D + V^k)$ -th order tensor satisfying $\sum_k \sum_{\mathbf{r} \in \Omega_{R^k}} \Phi_{i\mathbf{r}}^k = 1$. The derivation of the inequality is described in Proposition 1 in the supplementary material. The above lower bound can be decoupled into independent multiple many-body approximations for tensors $\mathcal{M}^1, \dots, \mathcal{M}^K$ where each tensor \mathcal{M}^k is defined as $\mathcal{M}_{i\mathbf{r}}^k = \mathcal{T}_i \Phi_{i\mathbf{r}}^k$, and an optimization problem for the mixture ratio $\eta = (\eta^1, \dots, \eta^K)$. More specifically, we decouple the lower bound as follows:

$$\bar{L}(\hat{\mathcal{Q}}, \Phi) = \sum_{k=1}^K L_{\text{MBA}}(\mathcal{M}^k; \mathcal{Q}^k) + J(\eta), \quad J(\eta) = \sum_{i \in \Omega_I} \sum_{k=1}^K \sum_{\mathbf{r} \in \Omega_{R^k}} \mathcal{T}_i \Phi_{i\mathbf{r}}^k \log \eta^k, \quad (9)$$

where the objective function of many-body approximation L_{MBA} is introduced in Equation (2). The EM algorithm iteratively optimizes the lower bound for tensors Φ during the E-step and tensors $\hat{\mathcal{Q}}$ during the M-step until convergence. Each step is a convex optimization while Equation (7) is a non-convex function. This procedure is guaranteed to converge, and each iteration increases the objective function (7) monotonically, which we prove in Theorem 4 in the supplementary material.

E-step We maximize the lower bound $\bar{L}(\hat{\mathcal{Q}}, \Phi)$ for Φ , that is,

$$\Phi = \arg \max_{\Phi \in \mathcal{D}} \bar{L}(\hat{\mathcal{Q}}, \Phi),$$

where the solution space \mathcal{D} is a set of K tensors such that each tensor is normalized by hidden variables, i.e., $\mathcal{D} = \{(\Phi^1, \dots, \Phi^K) \mid \sum_k \sum_{\mathbf{r} \in \Omega_{R^k}} \Phi_{i\mathbf{r}}^k = 1\}$. The optimal solution Φ^k is given as

$$\Phi_{i\mathbf{r}}^k = \frac{\hat{\mathcal{Q}}_{i\mathbf{r}}^k}{\sum_{k=1}^K \sum_{\mathbf{r} \in \Omega_{R^k}} \hat{\mathcal{Q}}_{i\mathbf{r}}^k}, \quad (10)$$

as shown in Proposition 2 in the supplementary material. The denominator in (10) is equivalent to the definition of the model \mathcal{P} .

M-step We maximize the lower bound for tensors $\mathcal{Q} = (\mathcal{Q}^1, \dots, \mathcal{Q}^K)$ and non-negative values η . Since the lower bound can be decoupled as shown in Equation (9), the required optimizations in the M-step are as follows:

$$\mathcal{Q}^k = \arg \max_{\mathcal{Q}^k \in \mathcal{B}^k} L_{\text{MBA}}(\mathcal{M}^k; \mathcal{Q}^k), \quad \eta = \arg \max_{0 \leq \eta^k \leq 1, \sum_k \eta^k = 1} J(\eta), \quad (11)$$

Algorithm 1: Non-negative Tensor Mixture Learning

input : Non-negative tensor \mathcal{T} , the number of mixtures K , and ranks (R^1, \dots, R^K)
Initialize \mathcal{Q}^k, η^k for all $k \in [K]$;
repeat
 $\mathcal{P}_i \leftarrow \sum_k \eta^k \mathcal{P}_i^k$ where $\mathcal{P}_i^k = \sum_{\mathbf{r} \in R^k} \mathcal{Q}_{i\mathbf{r}}^k$;
 $\mathcal{M}_{i\mathbf{r}}^k \leftarrow \mathcal{T}_i \mathcal{Q}_{i\mathbf{r}}^k / \mathcal{P}_i$ for all $k \in [K]$; // E-step
 Update tensor \mathcal{Q}^k for all $k \in [K]$ using Equations (1), (4), and (5); // M-step
 Update mixture ratio η^k using Equation (12) for all $k \in [K]$; // M-step
until *Convergence*;
return \mathcal{P}

where the model space \mathcal{B}^k is the set of low-body tensors corresponding to the k -th low-rank tensor \mathcal{P}^k . The naive implementation of the M-step requires a gradient method to solve the many-body approximation for \mathcal{M}^k . The existing algorithm for many-body approximation is based on the Natural gradient method [3], which requires cubic computational complexity for the number of parameters in the low-body tensor \mathcal{Q}^k . Thus, repeating the gradient method in each M-step is computationally expensive. However, we introduced the closed-form solution of the many-body approximation in Section 2.1, which eliminates the iterative gradient method in the M-step for Tucker and Train decomposition. We discuss more complicated low-rank structures in Section 3.3.

We also provide optimal updates for the mixture ratio η . By the condition $\partial J(\eta) / \partial \eta^k = 0$ and the normalizing condition $\sum_k \eta^k = 1$, the optimal η^k is simply given as follows:

$$\eta^k = \frac{\sum_{\mathbf{i} \in \Omega_I} \sum_{\mathbf{r} \in \Omega_{R^k}} \mathcal{M}_{i\mathbf{r}}^k}{\sum_{k=1}^K \sum_{\mathbf{i} \in \Omega_I} \sum_{\mathbf{r} \in \Omega_{R^k}} \mathcal{M}_{i\mathbf{r}}^k} \quad (12)$$

which are shown in Proposition 3 in the supplementary material. It is straightforward to check that the M-step is a convex optimization problem whatever the low-rank structure assumed on \mathcal{P}^k , given that we can decouple the lower bound into multiple independent convex many-body approximations.

While the EM-based method for CP decomposition optimizing KL divergence has already been developed in [12], our proposed framework addresses more general low-rank decompositions and their mixtures. We provide the entire algorithm in Algorithm 1. Notably, the framework does not require a learning rate that needs to be carefully tuned when relying on gradient-based methods.

EM tensor factorization for general non-negative tensors Non-negative tensor factorization optimizing KL divergence or cross-entropy is frequently used beyond density estimation and in various fields such as sound source separation [17], computer vision [15, 21], and data mining [6, 24]. Although the given tensor \mathcal{T} is not necessarily normalized in such applications, EM tensor factorization can be used for them as follows. First, we obtain the total sum of the input tensor $\mu = \sum_i \mathcal{T}_i$ and then perform EM tensor factorization on the normalized tensor \mathcal{T} by dividing all elements of \mathcal{T} by μ . Finally, all elements of the resulting mixture low-rank tensor are multiplied by μ . This procedure is justified by the property of the KL divergence, $D_{KL}(\mu\mathcal{P}, \mu\mathcal{T}) = \mu D_{KL}(\mathcal{P}, \mathcal{T})$, where μ is any non-negative value.

3.2 Analysis of computational complexity

In the following, we discuss the computational complexity of the proposed EM low-rank approximation without a mixture, specifically when $K = 1$. It is straightforward to see that the computational complexity for $K > 1$ is simply the sum of the complexity of each of the EM low-rank approximations used in the mixture.

In our proposed framework, we compute the sum over the visible variables $\mathbf{i} \in \Omega_I$ of the tensor \mathcal{M}^k in the M-step, using Equations (4), (5), and (12) for which the computational cost increases rapidly as the size of the tensor increases. However, if the input tensor \mathcal{T} is sparse, which is a reasonable assumption for most density estimation tasks, we can reduce the computational complexity of the summation because the tensor \mathcal{M}^k is also sparse for indices \mathbf{i} as the definition of $\mathcal{M}_{i\mathbf{r}}^k = \mathcal{T}_i \Phi_{i\mathbf{r}}^k$. More specifically, we replace the sum over the visible variables $\sum_{\mathbf{i} \in \Omega_I}$ with $\sum_{\mathbf{i} \in \Omega_I^o}$ where Ω_I^o is the set of

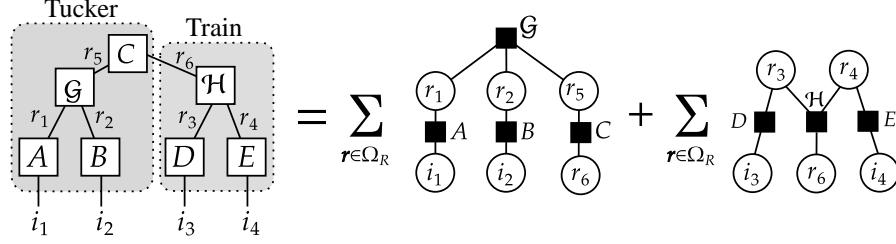


Figure 2: The M-step for the typical tensor tree structure is decomposed into two exactly solvable many-body approximations, which are enclosed by dotted lines.

indices of nonzero values of the tensor \mathcal{T} . The resulting time computational complexity is $O(\gamma NDR)$ for EM-CP decomposition and $O(\gamma DNR^D)$ for EM-Tucker and EM-Train decomposition where N is the number of nonzero values, D is the number of modes in the tensor, γ is the number of iteration, assuming ranks are (R, \dots, R) for all low-rank models.

Furthermore, the computational cost of the tensor train decomposition can be reduced to $O(\gamma DNR^2)$ by computing the sum over the latent variables $\mathbf{r} \in \Omega_R$ as follows. Firstly, we introduce the following tensors

$$\mathcal{G}_{i_1, \dots, i_d, r_d}^{(\rightarrow d)} = \sum_{r_{d-1}} \mathcal{G}_{i_1, \dots, i_{d-1}, r_{d-1}}^{(\rightarrow d-1)} \mathcal{G}_{r_{d-1} i_d r_d}^{(d)}, \quad \mathcal{G}_{i_{d+1}, \dots, i_D, r_d}^{(d\leftarrow)} = \sum_{r_{d+1}} \mathcal{G}_{r_d i_{d+1} r_{d+1}}^{(d+1)} \mathcal{G}_{i_{d+2}, \dots, i_D, r_{d+1}}^{(d+1\leftarrow)} \quad (13)$$

with $\mathcal{G}^{(\rightarrow 1)} = \mathcal{G}^{(1)}$, $\mathcal{G}^{(D-1\leftarrow)} = \mathcal{G}^{(D)}$, and $\mathcal{G}^{(\rightarrow 0)} = \mathcal{G}^{(D\leftarrow)} = 1$. Each complexity is $O(R_d)$ to get $\mathcal{G}^{(\rightarrow d)}$ and $\mathcal{G}^{(d\leftarrow)}$ when we compute them in the order of $\mathcal{G}^{(\rightarrow 2)}, \mathcal{G}^{(\rightarrow 3)}, \dots, \mathcal{G}^{(\rightarrow D)}$, and $\mathcal{G}^{(D-2\leftarrow)}, \mathcal{G}^{(D-3\leftarrow)}, \dots, \mathcal{G}^{(1\leftarrow)}$, respectively. The low-rank tensor \mathcal{P} also can be obtained with the cost $O(R_1)$ since it holds $\mathcal{P} = \mathcal{G}^{(\rightarrow D)} = \mathcal{G}^{(0\leftarrow)}$. Using these tensors, the update rule can be written as

$$\mathcal{G}_{r_{d-1} i_d r_d}^{(d)} = \frac{\sum_{\mathbf{i} \in \Omega_I^{\circ \setminus d}} \frac{\mathcal{T}_{\mathbf{i}}}{\mathcal{P}_{\mathbf{i}}} \mathcal{G}_{i_1, \dots, i_{d-1}, r_{d-1}}^{(\rightarrow d-1)} \mathcal{G}_{r_{d-1} i_d r_d}^{(d)} \mathcal{G}_{i_{d+1}, \dots, i_D, r_d}^{(d\leftarrow)}}{\sum_{\mathbf{i} \in \Omega_I^{\circ}} \frac{\mathcal{T}_{\mathbf{i}}}{\mathcal{P}_{\mathbf{i}}} \mathcal{G}_{i_1, \dots, i_d, r_d}^{(\rightarrow d)} \mathcal{G}_{i_{d+1}, \dots, i_D, r_d}^{(d\leftarrow)}} \quad (14)$$

for $\Omega_I^{\circ \setminus d} = \Omega_I^{\circ} \cap \Omega_I^{\setminus d}$. We used the relation $\mathcal{M}_{i\mathbf{r}} = \mathcal{T}_{\mathbf{i}} \Phi_{i\mathbf{r}}$ and $\Phi_{i\mathbf{r}} = \mathcal{Q}_{i\mathbf{r}} / \mathcal{P}_{\mathbf{i}}$ to get the above update rule. Not all elements in Equation (13) are necessary for updating tensors by Equation (14). We provide the EM-Train factorization in Algorithm 2 in the supplementary material.

Reordering tensor modes for EM-Train The tensor train decomposition results are influenced by the order of the modes in the tensor. To quantify the influence on and potentially enhance the performance of these tensor decompositions, we reorder the tensor modes based on normalized mutual information (NMI) between pairwise features in the data. We describe the definition of NMI in Section D.2 in the supplementary material. To illustrate this, we consider a dataset with five features. First, we select the two modes, j_1 and j_2 , with the highest NMI. These become the middle modes in the rearranged order. Next, we choose the mode j_3 with the second-highest NMI with j_1 , placing it to the left of j_1 . Then, we select the mode j_4 with the highest NMI with j_2 among the remaining unselected features (i.e., modes), placing it to the right of j_2 . This process is repeated until all features (modes) are selected, resulting in the tensor modes being rearranged from $(1, 2, 3, 4, 5)$ to $(j_5, j_3, j_1, j_2, j_4)$. The effectiveness of the reordering is examined in the supplementary material.

3.3 EM algorithm for more general low-rank structures

We now discuss how to find the solution for the many-body approximation required in the M-step when a more complex low-rank structure is assumed in the model. By the basic property of the logarithm function, the function L_{MBA} to be optimized in the M-step can be decoupled into independent solvable parts with closed form. As an example, we here see the tensor network state described in Figure 2, which is known as a typical tensor tree structure [18]. The objective function of many-body approximation in the M-step can be decoupled as follows:

$$\begin{aligned}
L_{\text{MBA}}(\mathcal{M}; \mathcal{Q}) &= \sum_{i \in \Omega_I} \sum_{\mathbf{r} \in \Omega_R} \mathcal{M}_{i\mathbf{r}} \log \mathcal{G}_{r_1 r_2 r_5} A_{i_1 r_1} B_{i_2 r_2} C_{r_5 r_6} D_{i_3 r_3} \mathcal{H}_{r_3 r_6 r_4} E_{r_4 i_4} \\
&= L_{\text{MBA}}(\mathcal{M}^{\text{Tucker}}; \mathcal{Q}^{\text{Tucker}}) + L_{\text{MBA}}(\mathcal{M}^{\text{Train}}; \mathcal{Q}^{\text{Train}})
\end{aligned} \tag{15}$$

where we define $\mathcal{M}_{i_1 i_2 r_1 r_2 r_5}^{\text{Tucker}} = \sum_{i_3 i_4 r_3 r_4 r_6} \mathcal{M}_{i\mathbf{r}}$ and $\mathcal{M}_{i_3 i_4 r_3 r_4 r_6}^{\text{Train}} = \sum_{i_1 i_2 r_1 r_2 r_5} \mathcal{M}_{i\mathbf{r}}$. We can optimize both terms in the final line by the closed-form solution introduced in Section 2.1. We provide theoretical support for this procedure, including normalization conditions, in Section D.1 in the supplementary material. By flexibly combining CP, Tucker, and Train decompositions, our EM-based framework can approximate tensors with a wide variety of low-rank structures.

3.4 Adaptive noise learning

Our general framework enables us to not only deal with typical low-rank structures and their mixture but also allow regularization and stabilization terms to be added to the model. For example, we here define model \mathcal{P} as the convex combination of a low-rank tensor $\mathcal{P}^{\text{low-rank}}$ and a normalized uniform tensor $\mathcal{P}^{\text{noise}}$ whose elements all are $1/|\Omega_I|$ as

$$\mathcal{P} = (1 - \eta^{\text{noise}}) \mathcal{P}^{\text{low-rank}} + \eta^{\text{noise}} \mathcal{P}^{\text{noise}},$$

where $|\Omega_I|$ is the number of elements of the input tensor \mathcal{T} , that is, $|\Omega_I| = I_1 I_2 \dots I_D$. The value η^{noise} indicates the magnitude of global shift or background noise in the data. This is a learnable parameter from the data, not a hyperparameter. It is obvious from the general theory of the EM algorithm described in Section 3.1 that the convexity of the E and M steps remain even in the presence of the noise term. We show in the next section by numerical experiments that the noise term is practically important for stabilization.

4 Numerical Experiments

We empirically examined the effectiveness of our framework using eight real-world categorical datasets. We downloaded these datasets from the repositories described in Table 5 and divided samples into 70% training, 15% validation, and 15% test samples to form train, validation, and test tensors, respectively. Each method decomposes the training tensor with ranks tuned such that the cross entropy between the reconstruction and the validation tensor is minimized. Performance was evaluated by the cross entropy between the reconstruction and the test tensor.

We compared our approach to the following baseline methods: Matrix Product States (MPS), Born Machine (BM), and Locally Purified State (LPS), which are also tensor-based methods [10]. The learning rate of the baseline methods was tuned so that the reconstruction tensor minimizes the KL divergence from the validation data.

Table 1: Negative log-likelihood per sample obtained on the test dataset.

	MPS	BM	LPS	CPTrainON
SolarFlare	6.54(0.14)	6.38(0.09)	6.35(0.06)	5.98(0.04)
Monk	6.63(0.26)	6.81(0.01)	6.56(0.23)	6.39(0.05)
SPECT	14.83(2.05)	12.04(0.44)	12.01(0.22)	11.60(0.27)
Lympho.	13.03(0.04)	12.34(0.20)	12.37(0.17)	12.13(0.35)
Votes	11.80(0.26)	10.64(0.38)	10.43(0.12)	10.37(0.04)
Hayesroth	5.20(1.01)	5.20(1.01)	4.71(0.01)	4.70(0.01)
Tumor	9.54(0.19)	9.28(0.17)	9.18(0.04)	9.11(0.04)
Chess2	10.38(0.01)	10.75(0.22)	10.40(0.00)	10.44(0.01)

In contrast, the proposed methods do not require a learning rate. We ran each of the procedures ten times with random initialization and reported mean values and the standard error in Table 1. Dataset details, experimental setup, and computational environment are described in detail in Section C. While the proposed framework can explore a variety of low-rank structures and their mixtures, we examine here the performance of CPTTrainON, a mixture of CP and Train decompositions with adaptive noise term and tensor mode re-ordering. The generalization performance of each model is shown in Table 1. We see that CPTTrainON has the best generalization performance on all datasets except Chess2. A more detailed comparison, including EMCP, can be found in Section B in the supplementary material.

Furthermore, we evaluated the validation error of the CP, Train, and Tucker decompositions including the adaptive noise term by varying the number of parameters in Figure 3. For the Tucker decomposition, we only considered three relatively small datasets, SolarFlare, Monk, and, Hayesroth,

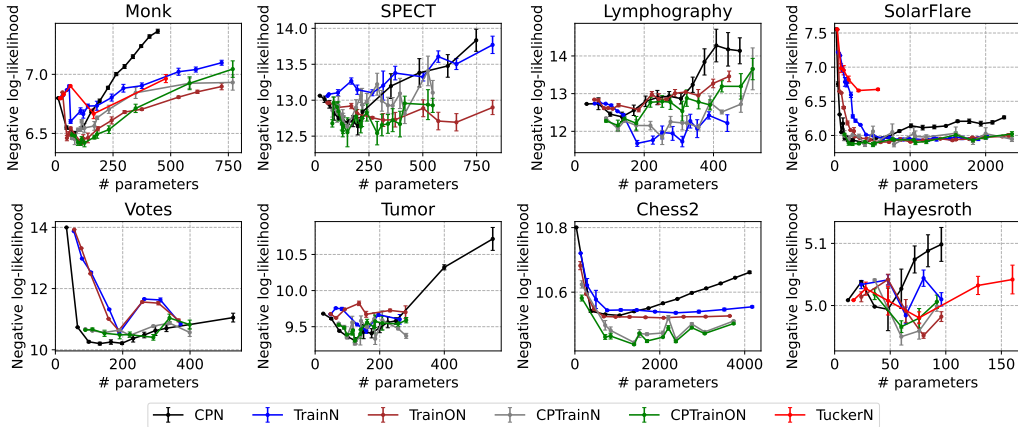


Figure 3: Validation error for each number of parameters for each method. The symbol ‘O’ indicates that the model includes mode reordering, and ‘N’ indicates that the model includes the noise term.

due to its high computational cost. No method alone shows superior performance on all datasets, however, we observe that the mixture of CP and Train generally performs well by combining the modeling capabilities of the two decomposition approaches. As a result, for Chess2, SolarFlare, Monk, and SPECT datasets, CPTrainON achieved the lowest validation error, while TrainN had the lowest validation error for Lymphography datasets, and CPN had the lowest error for Votes. Notably, our framework readily incorporates all these procedures providing a framework that allows decompositions with various low-rank structures and their combinations without tuning the learning rate.

We also compared the results using CPTrain with and without the adaptive noise term to verify its usefulness in Table 2. Although the noise term does not change the generalization performance significantly, we see in Figure 4 of the supplementary material that the models not including the adaptive noise term had significantly larger errors when the models were specified with large numbers of parameters and thus prone to overfitting. The full results of the experiment are given in Table 6 in the supplementary material.

Table 2: Generalization performance

	CPTrain	CPTrainN
SolarFlare	6.34(0.27)	5.98(0.06)
Monk	6.31(0.07)	6.43(0.07)
SPECT	11.22(0.11)	11.49(0.23)
Lympho.	22.13(11.02)	11.83(0.41)
Votes	11.13(0.65)	10.39(0.12)
Hayesroth	4.74(0.04)	4.76(0.00)
Tumor	9.28(0.14)	9.24(0.20)
Chess2	10.33(0.01)	10.44(0.01)

5 Conclusion

While it is a well-established principle that both real- and complex-valued tensors can be approximated with various low-rank structures based on local singular value decomposition (SVD), a unified framework for non-negative low-rank approximation has not been developed. Consequently, non-negative tensor factorizations typically require piecemeal tailored implementations that use gradient methods. This study introduces an EM-based unified framework that decouples the non-negative low-rank structure into multiple solvable many-body approximations and applies a closed-form solution locally, thereby eliminating the need for gradient methods. Our framework not only uniformly handles various low-rank structures but also supports adaptive noise terms and mixtures of low-rank tensors without losing the convergence guarantee. The flexibility of our modeling stems from the generality of the EM algorithm and a formulation that can take advantage of the logarithmic function properties that appear in the KL divergence. Empirical results demonstrate that our framework achieves superior generalization performance compared to baseline methods.

Limitations and broader impacts The proposed framework only works on non-negative tensors. The theoretical analysis supporting the generalization performance of the mixture models remains in future work. While this study discussed low-rank structures with tree structures, such as CP, Tucker, and Train decomposition, and their combinations, we did not discuss tensor networks with loops. Our work aims to establish a fundamental methodology for machine learning, and there is no direct risk of misuse or ethical issues. Please also see Section D.4 in the supplementary material.

References

- [1] (1987). Congressional Voting Records. UCI Machine Learning Repository. DOI: <https://doi.org/10.24432/C5C01P>.
- [2] (1989). Solar Flare. UCI Machine Learning Repository. DOI: <https://doi.org/10.24432/C5530G>.
- [3] Amari, S.-i. (2016). *Information geometry and its applications*, volume 194. Springer.
- [4] Bain, M. and Hoff, A. (1994). Chess (King-Rook vs. King). UCI Machine Learning Repository. DOI: <https://doi.org/10.24432/C57W2S>.
- [5] Cheng, S., Wang, L., Xiang, T., and Zhang, P. (2019). Tree tensor networks for generative modeling. *Phys. Rev. B*, 99:155131.
- [6] Chi, E. C. and Kolda, T. G. (2012). On tensors, sparsity, and nonnegative factorizations. *SIAM Journal on Matrix Analysis and Applications*, 33(4):1272–1299.
- [7] Dempster, A. P., Laird, N. M., and Rubin, D. B. (1977). Maximum likelihood from incomplete data via the EM algorithm. *Journal of the Royal Statistical Society*, 39(1):1–22.
- [8] Ghalamkari, K. and Sugiyama, M. (2021). Fast Tucker rank reduction for non-negative tensors using mean-field approximation. In *Advances in Neural Information Processing Systems*, volume 34, pages 443–454, Virtual Event.
- [9] Ghalamkari, K., Sugiyama, M., and Kawahara, Y. (2023). Many-body approximation for non-negative tensors. In *Advances in Neural Information Processing Systems*, volume 36, pages 257–292, New Orleans, US.
- [10] Glasser, I., Sweke, R., Pancotti, N., Eisert, J., and Cirac, I. (2019). Expressive power of tensor-network factorizations for probabilistic modeling. *Advances in neural information processing systems*, 32.
- [11] Hayes-Roth, B. and Hayes-Roth, F. (1989). Hayes-Roth. UCI Machine Learning Repository. DOI: <https://doi.org/10.24432/C5501T>.
- [12] Huang, K. and Sidiropoulos, N. D. (2017). Kullback-Leibler principal component for tensors is not NP-hard. In *2017 51st Asilomar Conference on Signals, Systems, and Computers*, pages 693–697. IEEE.
- [13] Iblisdir, S., Orus, R., and Latorre, J. (2007). Matrix product states algorithms and continuous systems. *Physical Review B*, 75(10):104305.
- [14] Jensen, J. L. W. V. (1906). Sur les fonctions convexes et les inégalités entre les valeurs moyennes. *Acta mathematica*, 30(1):175–193.
- [15] Kim, Y.-D., Cichocki, A., and Choi, S. (2008). Nonnegative Tucker decomposition with alpha-divergence. In *2008 IEEE International Conference on Acoustics, Speech and Signal Processing*, pages 1829–1832.
- [16] Kurgan, L. A., Cios, K. J., Tadeusiewicz, R., Ogiela, M., and Goodenday, L. S. (2001). Knowledge discovery approach to automated cardiac spect diagnosis. *Artificial intelligence in medicine*, 23(2):149–169.
- [17] Kırbız, S. and Günsel, B. (2014). A multiresolution non-negative tensor factorization approach for single channel sound source separation. *Signal Processing*, 105:56–69.
- [18] Liu, Y., Long, Z., and Zhu, C. (2018). Image completion using low tensor tree rank and total variation minimization. *IEEE Transactions on Multimedia*, 21(2):338–350.
- [19] Novikov, G. S., Panov, M. E., and Oseledets, I. V. (2021). Tensor-train density estimation. In *Uncertainty in artificial intelligence*, pages 1321–1331. PMLR.
- [20] Orús, R. (2014). A practical introduction to tensor networks: Matrix product states and projected entangled pair states. *Annals of Physics*, 349:117–158.

- [21] Phan, A. H. and Cichocki, A. (2008). Fast and efficient algorithms for nonnegative Tucker decomposition. In *Advances in Neural Networks-ISNN 2008: 5th International Symposium on Neural Networks, ISNN 2008, Beijing, China, September 24-28, 2008, Proceedings, Part II 5*, pages 772–782. Springer.
- [22] Silverman, B. W. (2018). *Density estimation for statistics and data analysis*. Routledge.
- [23] Strehl, A. and Ghosh, J. (2002). Cluster ensembles—a knowledge reuse framework for combining multiple partitions. *Journal of machine learning research*, 3(Dec):583–617.
- [24] Takeuchi, K., Tomioka, R., Ishiguro, K., Kimura, A., and Sawada, H. (2013). Non-negative multiple tensor factorization. In *2013 IEEE 13th International Conference on Data Mining*, pages 1199–1204. IEEE.
- [25] Thrun, S. (1991). The monk’s problems: A performance comparison of different learning algorithms. *Technical Report of Carnegie Mellon University*.
- [26] Tomczak, J. M. (2021). *Deep Generative Modeling*. Cham: Springer International Publishing.
- [27] Wu, C. J. (1983). On the convergence properties of the em algorithm. *The Annals of statistics*, pages 95–103.
- [28] Yang, Z., Zhang, H., Yuan, Z., and Oja, E. (2011). Kullback-leibler divergence for nonnegative matrix factorization. In *International Conference on Artificial Neural Networks*, pages 250–257. Springer.
- [29] Zwitter, M. and Soklic, M. (1988a). Lymphography. UCI Machine Learning Repository. DOI: <https://doi.org/10.24432/C54598>.
- [30] Zwitter, M. and Soklic, M. (1988b). Primary Tumor. UCI Machine Learning Repository. DOI: <https://doi.org/10.24432/C5WK5Q>.

Supplementary Material

Table of Contents

A Proofs	12
A.1 Proofs for exact solutions of many-body approximation	12
A.2 Proofs for EM-algorithm	15
B Additional experimental results	16
C Experimental details	18
C.1 Experimental setup	18
C.2 Implementation detail	19
C.3 Additional information for reproducibility	19
D Additional remarks	20
D.1 Technical detail for complicated low-rank structures	20
D.2 Definition of normalized mutual information	21
D.3 Notation, terminology, and evaluation metric	22
D.4 Limitations	22

A Proofs

A.1 Proofs for exact solutions of many-body approximation

First, we show the known solution formulas for the best CP rank-1 approximation that globally minimizes the KL divergence from the given tensor.

Theorem 1 (Optimal M-step in CP decomposition [12]). *For a given non-negative tensor $\mathcal{M} \in \mathbb{R}_{\geq 0}^{I_1 \times \dots \times I_D \times R}$, its many body approximation with interactions as described in Figure 1(a) is given as*

$$A_{i_{d^r}}^{(d)} = \frac{\sum_{i \in \Omega_I^d} \mathcal{M}_{ir}}{\mu^{1/D} \left(\sum_{i \in \Omega_I^d} \mathcal{M}_{ir} \right)^{1-1/D}}, \quad \mu = \sum_{i \in \Omega_I} \sum_{r \in \Omega_R} \mathcal{M}_{ir}$$

In the following, we provide proofs of the closed-form solutions of many-body approximation in Figure 1(b) and (c). When a factor in a low-body tensor is multiplied by ν , the value of the objective function of many-body approximation remains the same if another factor is multiplied by $1/\nu$, which we call the *scaling redundancy*. The key idea in the following proofs is reducing the scaling redundancy and absorbing the normalizing conditions of the entire tensor into a single factor. This enables the decoupling of the normalized condition of the entire tensor into independent conditions about factors. This trick is also used in Section D.1 to decouple more complicated low-rank structures into a combination of CP, Tucker, and Train decompositions.

Theorem 2 (The closed form of the optimal M-step in Tucker decomposition). *For a given tensor $\mathcal{M} \in \mathbb{R}_{\geq 0}^{I_1 \times \dots \times I_D \times R_1 \times \dots \times R_D}$, its many-body approximation with interaction described in Figure 1(b) is given as*

$$\mathcal{G}_r = \frac{\sum_{i \in \Omega_I} \mathcal{M}_{ir}}{\sum_{i \in \Omega_I} \sum_{r \in \Omega_R} \mathcal{M}_{ir}}, \quad A_{i_{d^r d}}^{(d)} = \frac{\sum_{i \in \Omega_I^d} \sum_{r \in \Omega_r^d} \mathcal{M}_{ir}}{\sum_{i \in \Omega_I} \sum_{r \in \Omega_R^d} \mathcal{M}_{ir}}.$$

Proof. The objective function of the many-body approximation is

$$L_{\text{MBA}}(\mathcal{M}; \mathcal{Q}^{\text{Tucker}}) = \sum_{i \in \Omega_I} \sum_{r \in \Omega_R} \mathcal{M}_{ir} \log \mathcal{Q}_{ir}^{\text{Tucker}} \quad (16)$$

where

$$Q_{i_1 \dots i_D r_1 \dots r_D}^{\text{Tucker}} = \mathcal{G}_{r_1 \dots r_D} A_{i_1 r_1}^{(1)} \dots A_{i_D r_D}^{(D)}.$$

Since many-body approximation parameterizes tensors as discrete probability distributions, we optimize the above objective function with normalizing condition $\sum_{i \in \Omega_I} \sum_{r \in \Omega_R} Q_{ir}^{\text{Tucker}} = 1$. Then, we consider the following Lagrange function:

$$\mathcal{L} = \sum_{i \in \Omega_I} \sum_{r \in \Omega_R} \mathcal{M}_{ir} \log \mathcal{G}_r A_{i_1 r_1}^{(1)} \dots A_{i_D r_D}^{(D)} - \lambda \left(\sum_{i \in \Omega_I} \sum_{r \in \Omega_R} \mathcal{G}_r A_{i_1 r_1}^{(1)} \dots A_{i_D r_D}^{(D)} - 1 \right)$$

To reduce the scaling redundancy and decouple the normalizing condition, we introduce scaled factor matrices $\tilde{A}^{(d)}$ as

$$\tilde{A}_{i_d r_d}^{(d)} = \frac{A_{i_d r_d}^{(d)}}{a_{r_d}^{(d)}}, \quad \text{where } a_{r_d}^{(d)} = \sum_{i_d} A_{i_d r_d}^{(d)}, \quad (17)$$

and the scaled core tensor,

$$\tilde{\mathcal{G}}_r = \mathcal{G}_r a_{r_1}^{(1)} \dots a_{r_D}^{(D)}.$$

The normalizing condition $\sum_{i \in \Omega_I} \sum_{r \in \Omega_R} Q_{ir}^{\text{Tucker}} = 1$ guarantees the normalization of the core tensor $\tilde{\mathcal{G}}$ as

$$\sum_{r \in \Omega_R} \tilde{\mathcal{G}}_r = 1. \quad (18)$$

The tensor Q^{Tucker} can be represented with the above introduced tensors as

$$Q_{ir}^{\text{Tucker}} = \mathcal{G}_r A_{i_1 r_1}^{(1)} \dots A_{i_D r_D}^{(D)} = \tilde{\mathcal{G}}_r \tilde{A}_{i_1 r_1}^{(1)} \dots \tilde{A}_{i_D r_D}^{(D)}.$$

We optimize $\tilde{\mathcal{G}}$ and $\tilde{A}_{i_d r_d}^{(d)}$ instead of \mathcal{G} and $A_{i_d r_d}^{(d)}$. Thus the Lagrange function can be written as

$$\mathcal{L} = \sum_{i \in \Omega_I} \sum_{r \in \Omega_R} \mathcal{M}_{ir} \log \tilde{\mathcal{G}}_r \tilde{A}_{i_1 r_1}^{(1)} \dots \tilde{A}_{i_D r_D}^{(D)} - \lambda \left(\sum_r \tilde{\mathcal{G}}_r - 1 \right) - \sum_{d=1}^D \sum_{r_d} \lambda_{r_d}^{(d)} \left(\sum_{i_d} \tilde{A}_{i_d r_d}^{(d)} - 1 \right). \quad (19)$$

The condition

$$\frac{\partial \mathcal{L}}{\partial \mathcal{G}_r} = \frac{\partial \mathcal{L}}{\partial A_{i_d r_d}^{(d)}} = 0$$

leads equations

$$\tilde{\mathcal{G}}_r = \frac{1}{\lambda} \sum_{i \in \Omega_I} \mathcal{M}_{ir}, \quad \tilde{A}_{i_d r_d}^{(d)} = \frac{1}{\lambda_d} \sum_{i \in \Omega_I \setminus i_d} \sum_{r \in \Omega_R \setminus r_d} \mathcal{M}_{ir}.$$

The values of Lagrange multipliers are identified by the normalizing conditions (17) and (18) as

$$\lambda = \sum_{i \in \Omega_I} \sum_{r \in \Omega_R} \mathcal{M}_{ir}, \quad \lambda_{r_d}^{(d)} = \sum_{i \in \Omega_I} \sum_{r \in \Omega_R \setminus r_d} \mathcal{M}_{ir}.$$

□

Theorem 3 (The closed form of the optimal M-step in Train decomposition). *For a given tensor $\mathcal{M} \in \mathbb{R}_{\geq 0}^{I_1 \times \dots \times I_D \times R_1 \times \dots \times R_{D-1}}$, its many-body approximation with interactions described in Figure 1(c) is given as*

$$\mathcal{G}_{r_{d-1} i_d r_d}^{(d)} = \frac{\sum_{i \in \Omega_I \setminus i_d} \sum_{r \in \Omega_R \setminus r_{d-1}} \mathcal{M}_{ir}}{\sum_{i \in \Omega_I} \sum_{r \in \Omega_R} \mathcal{M}_{ir}}$$

for $d = 1, \dots, D$, assuming $r_0 = r_D = 1$.

Proof. The objective function of the many-body approximation is

$$L_{\text{MBA}}(\mathcal{M}; \mathcal{Q}^{\text{Train}}) = \sum_{i \in \Omega_I} \sum_{\mathbf{r} \in \Omega_R} \mathcal{M}_{i\mathbf{r}} \log \mathcal{Q}_{i\mathbf{r}}^{\text{Train}}$$

where

$$\mathcal{Q}_{i_1 \dots i_D r_1 \dots r_D}^{\text{Train}} = \mathcal{G}_{i_1 r_1}^{(1)} \mathcal{G}_{r_1 i_2 r_2}^{(2)} \dots \mathcal{G}_{r_{D-1} i_D}^{(D)}$$

Since many-body approximation parameterizes tensors as discrete probability distributions, we optimize the above objective function with normalizing condition $\sum_{i \in \Omega_I} \sum_{\mathbf{r} \in \Omega_R} \mathcal{Q}_{i\mathbf{r}}^{\text{Train}} = 1$. Then, we consider the following Lagrange function:

$$\mathcal{L} = \sum_{i \in \Omega_I} \sum_{\mathbf{r} \in \Omega_R} \mathcal{M}_{i\mathbf{r}} \log \mathcal{G}_{i_1 r_1}^{(1)} \mathcal{G}_{r_1 i_2 r_2}^{(2)} \dots \mathcal{G}_{r_{D-1} i_D}^{(D)} - \lambda \left(\sum_{i \in \Omega_I} \sum_{\mathbf{r} \in \Omega_R} \mathcal{G}_{i_1 r_1}^{(1)} \mathcal{G}_{r_1 i_2 r_2}^{(2)} \dots \mathcal{G}_{r_{D-1} i_D}^{(D)} - 1 \right)$$

To decouple the normalizing condition and make the problem easier, we introduce scaled core tensors $\tilde{\mathcal{G}}^{(1)}, \dots, \tilde{\mathcal{G}}^{(D-1)}$ that are normalized over r_{d-1} and i_d as

$$\tilde{\mathcal{G}}_{r_{d-1} i_d r_d}^{(d)} = \frac{g_{r_{d-1}}^{(d-1)}}{g_{r_d}^{(d)}} \mathcal{G}_{r_{d-1} i_d r_d}^{(d)},$$

where we define

$$g_{r_d}^{(d)} = \sum_{r_{d-1}} \sum_{i_d} \mathcal{G}_{r_{d-1} i_d r_d}^{(d)} g_{r_{d-1}}^{(d-1)},$$

with $g_{r_0} = 1$. We assume $r_0 = r_D = 1$. Using the scaled core tensors, the tensor $\mathcal{Q}^{\text{Train}}$ can be written as

$$\mathcal{Q}_{i_1 \dots i_D r_1 \dots r_D}^{\text{Train}} = \mathcal{G}_{i_1 r_1}^{(1)} \mathcal{G}_{r_1 i_2 r_2}^{(2)} \dots \mathcal{G}_{r_{D-1} i_D}^{(D)} = \tilde{\mathcal{G}}_{i_1 r_1}^{(1)} \tilde{\mathcal{G}}_{r_1 i_2 r_2}^{(2)} \dots \tilde{\mathcal{G}}_{r_{D-1} i_D}^{(D)}$$

with

$$\tilde{\mathcal{G}}_{r_{D-1} i_D}^{(D)} = \frac{1}{g_{r_{D-1}}^{(D-1)}} \mathcal{G}_{r_{D-1} i_D}^{(D)}. \quad (20)$$

The matrix $\tilde{\mathcal{G}}^{(D)}$ is normalized, satisfying $\sum_{r_{D-1}} \sum_{i_D} \tilde{\mathcal{G}}_{r_{D-1} i_D}^{(D)} = 1$. Thus, the Lagrange function can be written as

$$\begin{aligned} \mathcal{L} = \sum_{i \in \Omega_I} \sum_{\mathbf{r} \in \Omega_R} \mathcal{M}_{i\mathbf{r}} \log \tilde{\mathcal{G}}_{i_1 r_1}^{(1)} \tilde{\mathcal{G}}_{r_1 i_2 r_2}^{(2)} \dots \tilde{\mathcal{G}}_{r_{D-1} i_D}^{(D)} - \sum_{d=1}^{D-1} \lambda_{r_d}^{(d)} \left(\sum_{r_{d-1}} \sum_{i_d} \tilde{\mathcal{G}}_{r_{d-1} i_d r_d}^{(d)} - 1 \right) \\ - \lambda^{(D)} \left(\sum_{r_{D-1}} \sum_{i_D} \tilde{\mathcal{G}}_{r_{D-1} i_D}^{(D)} - 1 \right). \end{aligned} \quad (21)$$

The critical condition

$$\frac{\partial \mathcal{L}}{\partial \mathcal{G}_{r_{d-1} i_d r_d}^{(d)}} = 0$$

leads the equation

$$\tilde{\mathcal{G}}_{r_{d-1} i_d r_d}^{(d)} = \frac{1}{\lambda_{r_d}^{(d)}} \sum_{i \in \Omega_I \setminus i_d} \sum_{\mathbf{r} \in \Omega_R \setminus r_{d-1}} \mathcal{M}_{i\mathbf{r}},$$

where the values of multipliers are identified by the normalizing conditions in Equation (20) as

$$\lambda_{r_d}^{(d)} = \sum_{i \in \Omega_I} \sum_{\mathbf{r} \in \Omega_R \setminus i_d} \mathcal{M}_{i\mathbf{r}}.$$

□

A.2 Proofs for EM-algorithm

We prove the propositions used to derive the EM algorithm for non-negative tensor mixture learning in Section 3. Furthermore, we show the convergence of the proposed method in Theorem 4.

Proposition 1. For any tensors Φ^1, \dots, Φ^K that satisfies $\sum_{k=1}^K \sum_{\mathbf{r} \in \Omega_{R^k}} \Phi_{i\mathbf{r}}^k = 1$, the cross entropy $L(\hat{\mathcal{Q}})$ in Equation (7) can be bounded as follows:

$$L(\hat{\mathcal{Q}}) \geq \bar{L}(\hat{\mathcal{Q}}, \Phi) = \sum_{i \in \Omega_I} \sum_{k=1}^K \sum_{\mathbf{r} \in \Omega_{R^k}} \mathcal{T}_i \Phi_{i\mathbf{r}}^k \log \frac{\hat{\mathcal{Q}}_{i\mathbf{r}}^k}{\Phi_{i\mathbf{r}}^k}.$$

Proof. For any tensors Φ^1, \dots, Φ^K that satisfies $\sum_{k=1}^K \sum_{\mathbf{r} \in \Omega_{R^k}} \Phi_{i\mathbf{r}}^k = 1$, we can transform the cross entropy $L(\hat{\mathcal{Q}})$ as follows:

$$\begin{aligned} L(\hat{\mathcal{Q}}) &= \sum_{i \in \Omega_I} \mathcal{T}_i \log \mathcal{P}_i \\ &= \sum_{i \in \Omega_I} \mathcal{T}_i \log \sum_{\mathbf{r} \in \Omega_{R^k}} \hat{\mathcal{Q}}_{i\mathbf{r}}^k \\ &= \sum_{i \in \Omega_I} \mathcal{T}_i \log \sum_{k=1}^K \sum_{\mathbf{r} \in \Omega_{R^k}} \frac{\Phi_{i\mathbf{r}}^k \hat{\mathcal{Q}}_{i\mathbf{r}}^k}{\Phi_{i\mathbf{r}}^k} \\ &\geq \sum_{i \in \Omega_I} \sum_{k=1}^K \sum_{\mathbf{r} \in \Omega_{R^k}} \mathcal{T}_i \Phi_{i\mathbf{r}}^k \log \frac{\hat{\mathcal{Q}}_{i\mathbf{r}}^k}{\Phi_{i\mathbf{r}}^k} = \bar{L}(\hat{\mathcal{Q}}, \Phi) \end{aligned}$$

where the following relation, called the Jensen inequality [14], is used:

$$f\left(\sum_{m=1}^M \lambda_m x_m\right) \leq \sum_{m=1}^M \lambda_m f(x_m) \quad (22)$$

for any convex function $f: \mathbb{R} \rightarrow \mathbb{R}$ and real numbers $\lambda_1, \dots, \lambda_M$ that satisfies $\sum_{m=1}^M \lambda_m = 1$. The inequality is adaptable because the logarithm function is a convex function. \square

Proposition 2. In E-step, the optimal update for Φ is given as

$$\tilde{\Phi}_{i\mathbf{r}}^k = \frac{\hat{\mathcal{Q}}_{i\mathbf{r}}^k}{\sum_{k=1}^K \sum_{\mathbf{r} \in \Omega_{R^k}} \hat{\mathcal{Q}}_{i\mathbf{r}}^k}.$$

Proof. We put Equation (10) into the lower bound \bar{L} in Equation (8),

$$\begin{aligned} \bar{L}(\hat{\mathcal{Q}}, \tilde{\Phi}) &= \sum_{i \in \Omega_I} \sum_{k=1}^K \sum_{\mathbf{r} \in \Omega_{R^k}} \mathcal{T}_i \tilde{\Phi}_{i\mathbf{r}}^k \log \frac{\hat{\mathcal{Q}}_{i\mathbf{r}}^k}{\tilde{\Phi}_{i\mathbf{r}}^k} \\ &= \sum_{i \in \Omega_I} \sum_{k=1}^K \sum_{\mathbf{r} \in \Omega_{R^k}} \mathcal{T}_i \frac{\hat{\mathcal{Q}}_{i\mathbf{r}}^k}{\sum_{k=1}^K \sum_{\mathbf{r} \in \Omega_{R^k}} \hat{\mathcal{Q}}_{i\mathbf{r}}^k} \log \sum_{k=1}^K \sum_{\mathbf{r} \in \Omega_{R^k}} \hat{\mathcal{Q}}_{i\mathbf{r}}^k \\ &= \sum_{i \in \Omega_I} \mathcal{T}_i \log \sum_{k=1}^K \sum_{\mathbf{r} \in \Omega_{R^k}} \hat{\mathcal{Q}}_{i\mathbf{r}}^k \\ &= L(\hat{\mathcal{Q}}). \end{aligned}$$

Jensen's inequality in Equation (22) shows that

$$L(\hat{\mathcal{Q}}) = \bar{L}(\hat{\mathcal{Q}}, \tilde{\Phi}) \geq \bar{L}(\hat{\mathcal{Q}}, \Phi) \quad (23)$$

for any tensors $\Phi \in \mathcal{D}$ where $\mathcal{D} = \{(\Phi^1, \dots, \Phi^K) \mid \sum_k \sum_{\mathbf{r} \in \Omega_{R^k}} \Phi_{i\mathbf{r}}^k = 1\}$. Thus, the tensors $\tilde{\Phi} = (\tilde{\Phi}^1, \dots, \tilde{\Phi}^K)$ are optimal. \square

Proposition 3. In M -step, the optimal update for η that optimizes $J(\eta)$ in Equation (9) is given as

$$\eta^k = \frac{\sum_{i \in \Omega_I} \sum_{r \in \Omega_{R^k}} \mathcal{T}_i \Phi_{i\mathbf{r}}^k}{\sum_{i \in \Omega_I} \sum_{k=1}^K \sum_{r \in \Omega_{R^k}} \mathcal{T}_i \Phi_{i\mathbf{r}}^k}$$

Proof. We optimize the decoupled objective function

$$J(\eta) = \sum_{i \in \Omega_I} \sum_{k=1}^K \sum_{r \in \Omega_{R^k}} \mathcal{T}_i \Phi_{i\mathbf{r}}^k \log \eta^k$$

with conditions $\sum_{k=1}^K \eta^k = 1$ and $\eta^k \geq 0$. Thus we consider the following Lagrange function

$$\mathcal{L} = \sum_{i \in \Omega_I} \sum_{k=1}^K \sum_{r \in \Omega_{R^k}} \mathcal{T}_i \Phi_{i\mathbf{r}}^k \log \eta^k - \lambda \left(\sum_{k=1}^K \eta^k - 1 \right)$$

The condition $\partial \mathcal{L} / \partial \eta^k = 0$ leads to

$$\eta^k = \frac{1}{\lambda} \sum_{i \in \Omega_I} \sum_{r \in \Omega_{R^k}} \mathcal{T}_i \Phi_{i\mathbf{r}}^k$$

where the normalization identifies the multiplier λ as

$$\lambda = \sum_{i \in \Omega_I} \sum_{k=1}^K \sum_{r \in \Omega_{R^k}} \mathcal{T}_i \Phi_{i\mathbf{r}}^k$$

□

Theorem 4. Mixture EM-tensor factorization always converges regardless of the choice of low-rank structure and mixtures.

Proof. We prove the convergence of the EM algorithm from the fact that the objective function L is bounded and that the E-step and M-step maximize the lower bound with respect to Φ and \hat{Q} , respectively. The E-step in iteration t updates Φ_{t-1} by optimal $\tilde{\Phi}_t$ to maximize the lower bound for Φ such as

$$L(\hat{Q}_t) = \bar{L}(\hat{Q}_t, \tilde{\Phi}_t) \geq \bar{L}(\hat{Q}_t, \Phi_{t-1}).$$

The M-step in iteration t updates \hat{Q}_t by \hat{Q}_{t+1} to maximize lower bound for \hat{Q} such as

$$\bar{L}(\hat{Q}_{t+1}, \tilde{\Phi}_t) \geq \bar{L}(\hat{Q}_t, \tilde{\Phi}_t).$$

Again, the E-step in iteration $t+1$ updates $\tilde{\Phi}_t$ by $\tilde{\Phi}_{t+1}$ to maximize lower bound for Φ such as

$$L(\hat{Q}_{t+1}) = \bar{L}(\hat{Q}_{t+1}, \tilde{\Phi}_{t+1}) \geq \bar{L}(\hat{Q}_{t+1}, \tilde{\Phi}_t).$$

Combining the above three relations, we get

$$L(\hat{Q}_{t+1}) = \bar{L}(\hat{Q}_{t+1}, \tilde{\Phi}_{t+1}) \geq \bar{L}(\hat{Q}_{t+1}, \tilde{\Phi}_t) \geq \bar{L}(\hat{Q}_t, \tilde{\Phi}_t) = L(\hat{Q}_t).$$

Thus, it holds that $L(\hat{Q}_{t+1}) \geq L(\hat{Q}_t)$. The algorithm converges because the cost function is bounded and monotonically increasing. □

B Additional experimental results

In this section, we discuss additional experimental results that could not be included in the main text due to page limitations.

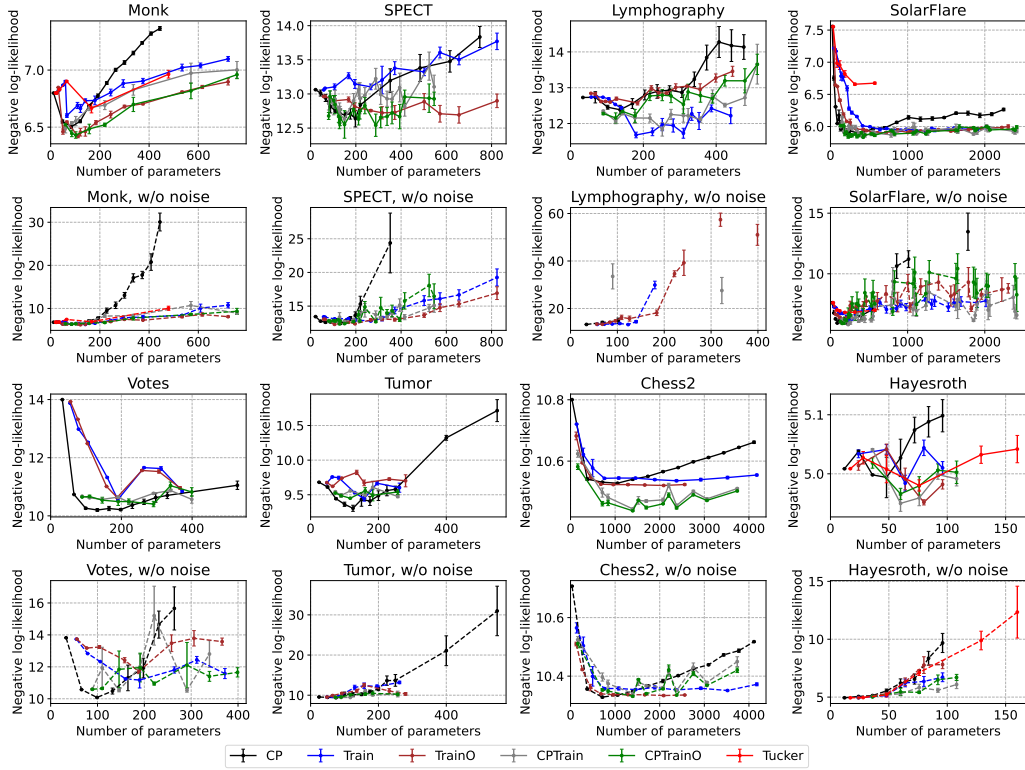


Figure 4: Validation error for each number of parameters for each dataset with adaptive noise learning (solid line) and without adaptive noise learning (dashed line).

Effect of the adaptive noise term We compare the validation error of the proposed model with and without the adaptive noise term in Figure 4. Focusing on the vertical axis, we can see that the validation errors for models without the adaptive noise term are huge where the number of parameters is large which makes the learning process unstable. Although the EM algorithms converge in theory, as shown in Theorem 4, the objective function often becomes NaN when the model has no adaptive noise term. This is because of numerical instability due to extremely small values in the logarithm function. The noise term, which adds values to all elements of the tensor, eliminates this problem. While adding a small uniform constant to values in a logarithmic function is often used as a heuristic to stabilize learning, our method provides a principled approach to learning such constant from the data.

Detailed comparison of EM-based methods We provide the comparison between Tucker and TuckerN in Table 3. We additionally provide the full results of the experiments in Table 6 to compare EM-based methods, including the exiting EMCP decomposition [12]. Interestingly, for some datasets, the simple EMCP shows the best generalization performance. However, as shown in Figure 4, EMCP without the noise term is prone to overfitting and, as a result, exhibits instability such that the value of the validation error increases rapidly when the number of parameters is large, i.e., the CP rank is large.

Table 3: Generalization performance

	Tucker	TuckerN
SolarFlare	6.78(0.15)	6.60(0.04)
Monk	6.80(0.00)	6.70(0.04)
Hayesroth	4.52(0.00)	4.62(0.00)

Direct comparison between MPS and EM-Train Both the proposed EMTrain and the baseline MPS are the same model, with different optimization methods. Although the ranks in both models are vector values, the official implementation of the MPS ² assumes that each element of the rank is the same while the rank of proposed methods has been tuned following the way described in Section C.2. Therefore, for a direct and more fair comparison, we have conducted our comparison experiments again fixing the range of train ranks for EMTrainN and EMTrainON to be (r, \dots, r) for $r = 1, \dots, 8$. The results are provided in Table 4 where we again observe that EMTrainON outperforms MPS for all datasets except Chess2.

Table 4: Generalization performance

	MPS	TrainN	TrainON
SolarFlare	6.54(0.14)	6.02 (0.04)	6.07(0.06)
Monk	6.63(0.26)	6.66(0.10)	6.43 (0.07)
SPECT	14.83(2.05)	12.08(0.00)	11.22 (0.11)
Lymphography	13.03(0.04)	12.69(0.19)	12.10 (0.12)
Votes	11.80(0.26)	10.31 (0.04)	10.56(0.16)
Hayesroth	5.20(1.01)	4.94(0.06)	4.85 (0.06)
Tumor	9.54(0.19)	9.23 (0.11)	9.52(0.00)
Chess2	10.38 (0.01)	10.54(0.01)	10.52(0.01)

C Experimental details

C.1 Experimental setup

We download six categorical tabular datasets SolarFlare, Monk, SPECT, Lymphography, Hayesroth, and Chess2 from the UCI database,¹ none of which contain any missing values, and two preprocessed categorical tabular datasets Votes and Tumor from the official repository of baselines [10]. All these datasets, except Hayesroth and Chess2, are used in the paper of the baseline methods [10]. Each dataset contains N categorical samples $x_n = (i_1, \dots, i_D)$. Both the number of samples, N , and the sample dimension, D , vary across datasets as seen in Table 5. In the original datasets, each i_d represents a categorical quantity such as color, location, gender, etc. By mapping these to natural numbers, each feature i_d is converted to a natural number from 1 to I_d , where I_d is the degree of freedom in the d -th feature. We randomly select 70% of the N samples to create the training index set Ω^{train} , 15% of samples to create the validation index set Ω^{valid} , and the final 15% of the samples form the test index set Ω^{test} . Some datasets may contain exactly the same samples. To deal with such datasets, we suppose that these indices sets may contain multiple identical elements.

We create empirical tensors $\mathcal{T}^{\text{train}}$, $\mathcal{T}^{\text{valid}}$, and $\mathcal{T}^{\text{test}}$, where each value \mathcal{T}_i^ℓ is defined as the number of i in the set Ω^ℓ for $\ell \in \{\text{train, valid, test}\}$. They are typically very sparse tensors. The above procedure to create empirical tensors is consistent with the discussion at the beginning of Section 3. We normalize each tensor by dividing all the elements by the sum of the tensor to map them to a discrete probability distribution.

During the training phase, by optimizing the log-likelihood

$$D(\mathcal{T}^{\text{train}}, \mathcal{P}) = \sum_{i \in \Omega^{\text{train}}} \mathcal{T}_i^{\text{train}} \log \mathcal{P}_i,$$

we decompose the tensor $\mathcal{T}^{\text{train}}$ to obtain the reconstructed tensor \mathcal{P} , which approximates $\mathcal{T}^{\text{train}}$. We adjust hyper-parameters such as tensor ranks, bounds, and learning rates to minimize the distance $D(\mathcal{T}^{\text{valid}}, \mathcal{P})$. Finally, we evaluate the generalization error $D(\mathcal{T}^{\text{test}}, \mathcal{P})$, where \mathcal{P} is the reconstruction approximating $\mathcal{T}^{\text{train}}$ with tuned rank. The proposed method and the baseline method have initial value dependence. Hence, all calculations were repeated five times to evaluate the mean and standard deviation of the cross-entropy.

¹<https://archive.ics.uci.edu/>,

Table 5: Datasets used in experiments. The sparsity of dataset is defined as $N/|\Omega_I|$.

	# Feature D	# Non-zero values N	Tensor size $ \Omega_I $	Sparsity $N/ \Omega_I $	
Solarflare [2]	9	1067	41472	0.0257	Link
Monks [25]	7	432	864	0.5000	Link
SPECT [16]	23	267	4194304	1.7e-04	Link
Lymphography [29]	18	148	113246208	1.3e-06	Link
Votes [1]	17	376	86093442	4.4e-6	Link
Hayesroth [11]	5	160	256	0.6250	Link
Tumor [30]	17	301	2654208	1.1e-4	Link
Chess2 [4]	6	25057	65536	0.382	Link

C.2 Implementation detail

We describe the implementation details of methods in the following. All methods are implemented in Python 3.12.3. For reproducibility, we provide our source code for all experiments in the supplementary material.

Proposed method The pseudocodes are described in Algorithms 1 and 2. All tensors and mixture ratios were initialized with a uniform distribution between 0 and 1 and normalized as necessary. The algorithm was terminated when the number of iterations of the EM step exceeded 1200 or when the difference of the log-likelihood from the previous iteration was below $10e-6$. The source code used in the experiments is available in the supplementary material. We manually determined the values of the ranks to be searched for each dataset so ensure that we observe underfitting, better fitting, and overfitting regimes for each validation dataset. In the EM tensor-train model, ranks of the central core tensors are adjusted to be equal to or larger than the ranks of the core tensors at the edges. This is because modes with large mutual information are gathered in the center of the train-structure due to reordering. The searched rank ranges are available in `exp_config.py` in the supplementary material. To reorder tensor modes, we use the greedy method, which can be found in `MI.py` in the supplementary material.

Baselines We downloaded the source code for Positive Matrix Product State (MPS), Real Born Machine (BM), and Real Locally Purified State (LPS) from the official repository.² The license of the code is described in the repository as MIT License. We varied the learning rates from $1.0e-4$, $1.0e-3$, ... to $1.0e+4$ for training data. We then used the learning rate that yielded the smallest validation score. According to the description in the README file, the batch size was fixed at 20, and the number of iterations was set to 20,000. We performed 5 experiments at each bond and evaluated the mean and standard deviation. We varied the bond of the model from 1, 2, ... to 8, and evaluated the test data with the bond value that best fit the validation data.

C.3 Additional information for reproducibility

Environment Experiments were conducted on Ubuntu 20.04.1 with a single core of 2.1GHz Intel Xeon CPU Gold 5218 and 128GB of memory. This work does not require GPU computing. The total computation time for all experiments, including tuning the learning rate of the baselines, was less than 240 hours, using 88 threads of parallel computing.

Dataset detail, license, and availability We downloaded real-world datasets described in Table 5 through the Python package `ucimlrepo`. All of these datasets are licensed under a Creative Commons Attribution 4.0 International (CC BY 4.0) license, as seen on each web page in the UCI database.¹ The imported data were directly converted to tensors by the procedure described in Section C.1. For the Monk dataset, we concatenate targets and features to make the data sparser, which is shown in `prepro.py` in the supplementary material.

²https://github.com/glivan/tensor_networks_for_probabilistic_modeling,

D Additional remarks

D.1 Technical detail for complicated low-rank structures

We decoupled the tensor many-body decomposition into independent problems in Section 3.3 using the basic property of logarithmic functions. We show here that the normalization for the model is satisfied when we use the solution formula of the many-body approximation for each decoupled problem.

In the following, we discuss the decomposition as described in Figure 2 as an example, while the generalization to arbitrary tree low-rank structures is straightforward. When we decouple the many-body approximation in Equation (15) into the many-body approximation corresponding to the Tucker and Train decompositions, we need to guarantee that the normalizing condition

$$\sum_{i \in \Omega_I} \sum_{r \in \Omega_R} Q_{ir} = 1 \quad (24)$$

is satisfied where we define

$$Q_{ir} = \mathcal{G}_{r_1 r_2 r_5} A_{i_1 r_1} B_{i_2 r_2} C_{r_5 r_6} D_{i_3 r_3} \mathcal{H}_{r_3 r_6 r_4} E_{r_4 i_4}. \quad (25)$$

As explained at the beginning of Section A.1, we reduce scaling redundancy by normalizing each factor and decomposing the Lagrange function into independent parts. More specifically, we define a single root tensor and introduce normalized factors that sums over the edges that lie below from the root. Although the choice of the root tensor is not unique, we let tensor \mathcal{G} be the root tensor and introduce

$$\tilde{A}_{i_1 r_1} = \frac{1}{a_{r_1}} A_{i_1 r_1}, \quad \tilde{B}_{i_2 r_2} = \frac{1}{b_{r_2}} B_{i_2 r_2}, \quad \tilde{C}_{r_5 r_6} = \frac{h_{r_6}}{c_{r_5}} C_{r_5 r_6}, \quad (26)$$

$$\tilde{D}_{i_3 r_3} = \frac{1}{d_{r_3}} D_{i_3 r_3}, \quad \tilde{E}_{i_4 r_4} = \frac{1}{e_{r_4}} E_{i_4 r_4}, \quad \tilde{\mathcal{H}}_{r_3 r_4 r_6} = \frac{d_{r_3} e_{r_4}}{h_{r_6}} \mathcal{H}_{r_3 r_4 r_6} \quad (27)$$

where each normalizer is defined as

$$a_{r_1} = \sum_{i_1} A_{i_1 r_1}, \quad b_{r_2} = \sum_{i_2} B_{i_2 r_2}, \quad c_{r_5} = \sum_{r_6} C_{r_5 r_6} h_{r_6},$$

$$d_{r_3} = \sum_{i_3} D_{i_3 r_3}, \quad e_{r_4} = \sum_{i_4} E_{i_4 r_4}, \quad h_{r_6} = \sum_{r_3 r_4} d_{r_3} e_{r_4} \mathcal{H}_{r_3 r_4 r_6},$$

then it holds that

$$\sum_{i_1} \tilde{A}_{i_1 r_1} = \sum_{i_2} \tilde{B}_{i_2 r_2} = \sum_{r_6} \tilde{C}_{r_5 r_6} = \sum_{i_3} \tilde{D}_{i_3 r_3} = \sum_{i_4} \tilde{E}_{i_4 r_4} = \sum_{r_3 r_4} \tilde{\mathcal{H}}_{r_3 r_4 r_6} = 1.$$

We define the tensor $\tilde{\mathcal{G}}$ as $\tilde{\mathcal{G}}_{r_1 r_2 r_5} = a_{r_1} b_{r_2} c_{r_5} \mathcal{G}_{r_1 r_2 r_5}$ and putting Equations (26) and (27) into Equations (25) and (24), we obtain the condition for the root tensor \mathcal{G} as

$$\sum_{r_1 r_2 r_5} \tilde{\mathcal{G}}_{r_1 r_2 r_5} = 1.$$

Then, the tensor \mathcal{Q} can be written as

$$Q_{ir} = \tilde{\mathcal{G}}_{r_1 r_2 r_5} \tilde{A}_{i_1 r_1} \tilde{B}_{i_2 r_2} \tilde{C}_{r_5 r_6} \tilde{D}_{i_3 r_3} \tilde{\mathcal{H}}_{r_3 r_6 r_4} \tilde{E}_{r_4 i_4}. \quad (28)$$

The above approach to reduce scaling redundancy is illustrated in Figure 5. Finally, the original optimization problem with the Lagrange function

$$\mathcal{L} = \sum_{i \in \Omega_I} \sum_{r \in \Omega_R} \mathcal{M}_{ir} \log Q_{ir} - \lambda \left(1 - \sum_{i \in \Omega_I} \sum_{r \in \Omega_R} Q_{ir} \right)$$

is equivalent to the problem with the Lagrange function

$$\mathcal{L} = \mathcal{L}^{\text{Tucker}} + \mathcal{L}^{\text{Train}}$$

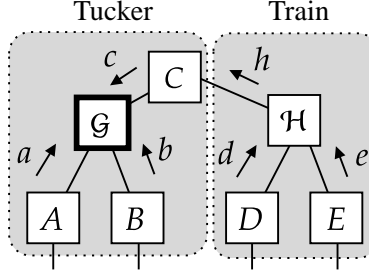


Figure 5: We normalize all tensors except for the root tensor, which is enclosed in a bold line. We then push the normalizer of each tensor, $a, b, c, d, e,$ and h on the root tensor. The root tensor absorbs scaling redundancy. This procedure decouples the Lagrangian into two independent problems.

where

$$\begin{aligned} \mathcal{L}^{\text{Tucker}} = & \sum_{\mathbf{i} \in \Omega_I} \sum_{\mathbf{r} \in \Omega_R} \mathcal{M}_{\mathbf{i}\mathbf{r}} \log \tilde{G}_{r_1 r_2 r_5} \tilde{A}_{i_1 r_1} \tilde{B}_{i_2 r_2} \tilde{C}_{r_5 r_6} + \lambda^{\mathcal{G}} \left(\sum_{r_1 r_2 r_5} \tilde{G}_{r_1 r_2 r_5} - 1 \right) \\ & + \sum_{r_1} \lambda_{r_1}^A \left(\sum_{i_1} \tilde{A}_{i_1 r_1} - 1 \right) + \sum_{r_2} \lambda_{r_2}^B \left(\sum_{i_2} \tilde{B}_{i_2 r_2} - 1 \right) + \sum_{r_5} \lambda_{r_5}^C \left(\sum_{r_6} \tilde{C}_{r_5 r_6} - 1 \right), \end{aligned}$$

which is equivalent to the Lagrange function for the Tucker decomposition given in Equation (19) and

$$\begin{aligned} \mathcal{L}^{\text{Train}} = & \sum_{\mathbf{i} \in \Omega_I} \sum_{\mathbf{r} \in \Omega_R} \mathcal{M}_{\mathbf{i}\mathbf{r}} \log \tilde{\mathcal{H}}_{r_3 r_4 r_6} \tilde{D}_{i_3 r_3} \tilde{E}_{i_4 r_4} \\ & + \sum_{r_3} \lambda_{r_3}^D \left(\sum_{i_3} \tilde{D}_{i_3 r_3} - 1 \right) + \sum_{r_4} \lambda_{r_4}^E \left(\sum_{i_4} \tilde{E}_{i_4 r_4} - 1 \right) + \sum_{r_6} \lambda_{r_6}^{\mathcal{H}} \left(\sum_{r_3 r_4} \tilde{\mathcal{H}}_{r_3 r_4 r_6} - 1 \right), \end{aligned}$$

which is also equivalent to the Lagrange function for the Train decomposition given in Equation (21) assuming $G^{(D)}$ is a normalized uniform tensor. For simplicity, we define tensors

$$\mathcal{M}_{i_1 i_2 r_1 r_2 r_5}^{\text{Tucker}} = \sum_{i_3 i_4} \sum_{r_3 r_4 r_6} \mathcal{M}_{\mathbf{i}\mathbf{r}}, \quad \mathcal{M}_{i_3 i_4 r_3 r_4 r_6}^{\text{Train}} = \sum_{i_1 i_2} \sum_{r_1 r_2 r_5} \mathcal{M}_{\mathbf{i}\mathbf{r}},$$

then, solve these independent many-body approximations by the closed-form solution by Equations (4) and (5) for given tensors $\mathcal{M}^{\text{Tucker}}$ and $\mathcal{M}^{\text{Train}}$, respectively, and multiply solutions to get optimal tensor \mathcal{Q} as Equation (28), which satisfied the normalizing condition in Equation (24).

D.2 Definition of normalized mutual information

This section describes the definition of the mutual information [23] used in the paper. For a given normalized non-negative tensor $\mathcal{T} \in \mathbb{R}_{\geq 0}^{I_1 \times \dots \times I_D}$, we define its normalized mutual information between two modes $d, l \in [D]$ as

$$\mathbb{H}_{d,l} = \frac{\mathbb{I}_{d,l}}{\sqrt{\mathbb{H}_d \mathbb{H}_l}}$$

where mutual information $\mathbb{I} \in \mathbb{R}^{D \times D}$ and individual entropy $\mathbb{H} \in \mathbb{R}^D$ are defined as

$$\mathbb{I}_{d,l} = \sum_{i_d, i_l} \mathcal{T}_{i_d i_l}^{(d,l)} \log \frac{\mathcal{T}_{i_d i_l}^{(d,l)}}{\mathcal{T}_{i_d}^{(d)} \mathcal{T}_{i_l}^{(l)}}, \quad \mathbb{H}_d = \sum_{i_d} \mathcal{T}_{i_d}^{(d)} \log \mathcal{T}_{i_d}^{(d)}$$

for marginalized tensors

$$\mathcal{T}_{i_d i_l}^{(d,l)} = \sum_{\mathbf{i} \in \Omega_I^{d,l}} \mathcal{T}_{\mathbf{i}}, \quad \mathcal{T}_{i_d}^{(d)} = \sum_{\mathbf{i} \in \Omega_I^d} \mathcal{T}_{\mathbf{i}}.$$

Algorithm 2: EM Train decomposition

input : Non-negative tensor \mathcal{T} and train rank $R^{\text{Train}} = (R_1, \dots, R_{D-1})$.
Initialize $\mathcal{Q}^{\text{Train}}$;
repeat
 $\mathcal{M}_{ir}^{\text{Train}} \leftarrow \mathcal{T}_i \mathcal{Q}_{ir}^{\text{Train}} / \mathcal{P}_i^{\text{Train}}$ for $i \in \Omega_I^o$; // E-step
 for $d \leftarrow 1$ **to** D **do**
 Obtain $\mathcal{G}^{(\rightarrow d)}$ and $\mathcal{G}^{(D-d \leftarrow)}$ using Equation (13);
 Update $\mathcal{G}^{(1)}, \dots, \mathcal{G}^{(D)}$ using Equation (14);
 $\mathcal{P}_i^{\text{Train}} \leftarrow \mathcal{G}_i^{(\rightarrow D)}$ for $i \in \Omega_I^o$;
until *Convergence*;
return $\mathcal{G}^{(1)}, \dots, \mathcal{G}^{(D)}$

D.3 Notation, terminology, and evaluation metric

Although all symbols and technical terms are properly introduced in the main text, we provide our notation here for readability.

The symbol $\mathbb{R}_{\geq 0}$ denotes the set of non-negative real numbers. The set of all natural numbers less than or equal to a natural number K is denoted by $[K]$. We use the Landau symbol O for computational time complexity.

Tensors We refer to a tensor whose elements all are nonnegative as a nonnegative tensor. The number of axes of a tensor is called its modes. The number of modes is called the order. For example, a vector is a first-order tensor, and a matrix is a second-order tensor. Tensors are denoted by calligraphic capital letters, as $\mathcal{T}, \mathcal{P}, \mathcal{Q}, \mathcal{M}, \dots$. A non-negative tensor whose sum over all indices is 1 is called a normalized tensor. Tensors and matrices whose sums over some indices equal 1 are marked with a tilde as $\tilde{\mathcal{Q}}$. Although the beginning and last core tensors of the tensor-train format are matrices rather than tensors, they are denoted by the calligraphic form $\mathcal{G}^{(1)}$ and $\mathcal{G}^{(D)}$ for notational convenience. The element-wise product of a normalized non-negative tensor \mathcal{Q}^k and a weight η^k is written with a hat, e.g., $\hat{\mathcal{Q}}^k = \eta^k \mathcal{Q}^k$.

EM algorithm The solution spaces for the E and M steps are represented by \mathcal{D} and \mathcal{B} , respectively. Since the solution space of the M-step is equivalent to that of the many-body approximation for tensors, we use \mathcal{B} to denote both. The objective function of the EM algorithm is L , and its lower bound is written using overlined L as \bar{L} .

Indices The visible variables $\mathbf{i} = (i_1, \dots, i_D)$ and hidden variables $\mathbf{r} = (r_1, \dots, r_V)$ are denoted as lower subscripts. The index set of visible variables and hidden variables are denoted as Ω_I and Ω_R , respectively. Multiple tensors are represented using superscripts with parentheses, such as $\mathcal{G}^{(1)}, \dots, \mathcal{G}^{(D)}$. Indices for mixtures are expressed as superscripts without parentheses. For example, the mixing ratio is represented by $\eta = (\eta^1, \dots, \eta^K)$. The symbol Ω_I^o is for the set of indices of nonzero values of the tensor \mathcal{T} , that is, $\Omega_I^o = \{\mathbf{i} \mid \mathcal{T}_{\mathbf{i}} \neq 0\} \subseteq \Omega_I$.

Metric The proposed framework and baselines optimize the KL divergence between tensors [28], which is defined as

$$D_{KL}(\mathcal{T}, \mathcal{P}) = \sum_{\mathbf{i} \in \Omega_I} \left\{ \mathcal{T}_{\mathbf{i}} \log \frac{\mathcal{T}_{\mathbf{i}}}{\mathcal{P}_{\mathbf{i}}} - \mathcal{T}_{\mathbf{i}} + \mathcal{P}_{\mathbf{i}} \right\}$$

where \mathcal{T} and \mathcal{P} can be non-normalized or normalized tensors. For a given tensor \mathcal{T} , the optimization of the KL divergence for the tensor \mathcal{P} is equivalent to the maximization of the cross-entropy, which is also equivalent to minimizing the negative log-likelihood per sample.

D.4 Limitations

In addition to the description in Section 5, the limitations are further discussed below. We have empirically examined the effectiveness of the proposed method only for discrete density estimation.

The method cannot be used directly in situations where there are missing values in the data. The number of ranks that need to be tuned is larger in mixture models than in the non-mixture low-rank model. The method to decouple a complicated low-rank structure into solvable CP, Tucker, and Train decompositions is not unique. Thus, establishing an efficient decoupling method is also a subject for future work.

Table 6: Negative log-likelihood per sample obtained on the test dataset. The symbol O means that the model includes mode reordering and N means the model includes the adaptive noise term.

	CP	CPN	Train	TrainN	TrainO	TrainON	CPTrain	CPTrainN	CPTrainO	CPTrainON
SolarFlare	6.04(0.19)	5.95(0.02)	6.07(0.05)	6.02(0.06)	6.13(0.02)	6.06(0.05)	6.34(0.27)	5.98(0.06)	6.54(0.73)	5.98(0.04)
Monk	6.29(0.10)	6.49(0.08)	6.40(0.35)	6.72(0.10)	6.57(0.32)	6.39(0.07)	6.31(0.07)	6.43(0.07)	6.36(0.11)	6.39(0.05)
SPECT	11.28(0.56)	11.46(0.19)	12.67(1.15)	12.08(0.00)	11.60(0.08)	11.67(0.12)	11.22(0.11)	11.49(0.23)	11.35(0.00)	11.60(0.27)
Lympho.	13.02(0.00)	12.58(0.00)	17.34(3.20)	12.86(0.11)	13.53(1.24)	12.21(0.13)	22.13(11.02)	11.83(0.41)	inf(nan)	12.13(0.35)
Votes	10.83(0.43)	10.34(0.07)	11.98(2.01)	10.30(0.02)	12.86(0.90)	10.49(0.01)	11.13(0.65)	10.39(0.12)	17.26(14.42)	10.37(0.04)
Hayesroth	4.52(0.00)	4.84(0.03)	4.56(0.02)	4.86(0.05)	4.48(0.06)	4.74(0.06)	4.74(0.04)	4.76(0.00)	4.65(0.01)	4.70(0.01)
Tumor	9.11(0.02)	9.21(0.06)	9.39(0.00)	9.23(0.12)	9.38(0.00)	9.51(0.01)	9.28(0.14)	9.24(0.20)	9.13(0.08)	9.11(0.04)
Chess2	10.33(0.01)	10.53(0.01)	10.35(0.01)	10.54(0.01)	10.33(0.01)	10.52(0.01)	10.33(0.00)	10.44(0.01)	10.33(0.00)	10.44(0.01)

